Experimental Eye Research 209 (2021) 108687

Contents lists available at ScienceDirect

Experimental Eye Research

journal homepage: www.elsevier.com/locate/yexer

Antimycin A-induced mitochondrial dysfunction regulates inflammasome signaling in human retinal pigment epithelial cells

Eveliina Korhonen [a,b,*], Maria Hytti [a], Niina Piippo [a], Kai Kaarniranta [c,d], Anu Kauppinen [a,**]

[a] Immuno-Ophthalmology, School of Pharmacy, Faculty of Health Sciences, University of Eastern Finland, P.O.Box 1627, FI-70211, Kuopio, Finland
[b] Department of Clinical Chemistry, University of Helsinki and Helsinki University Hospital, P.O.Box 720, FI-00029, Helsinki, Finland
[c] Department of Ophthalmology, Institute of Clinical Medicine, University of Eastern Finland, P.O.Box 1627, FI-70211, Kuopio, Finland
[d] Department of Ophthalmology, Kuopio University Hospital, P.O.Box 100, FI-70029, Kuopio, Finland

ARTICLE INFO

Keywords:
Age-related macular degeneration
Retinal pigment epithelium
AIM2
NLRP3
Inflammasome
Interleukin-1beta
Mitochondrial damage

ABSTRACT

Age-related macular degeneration (AMD) is a severe retinal eye disease where dysfunctional mitochondria and damaged mitochondrial DNA in retinal pigment epithelium (RPE) have been demonstrated to underlie the pathogenesis of this devastating disease. In the present study, we aimed to examine whether damaged mitochondria induce inflammasome activation in human RPE cells. Therefore, ARPE-19 cells were primed with IL-1α and exposed to the mitochondrial electron transport chain complex III inhibitor, antimycin A. We found that antimycin A-induced mitochondrial dysfunction caused caspase-1-dependent inflammasome activation and subsequent production of mature IL-1β and IL-18 in human RPE cells. AIM2 and NLRP3 appeared to be the responsible inflammasome receptors upon antimycin A-induced mitochondrial damage. We aimed at verifying our findings using hESC-RPE cells but antimycin A was absorbed by melanin. Therefore, results were repeated on D407 RPE cell cultures. Antimycin A-induced mitochondrial and NADPH oxidase-dependent ROS production occurred upstream of inflammasome activation, whereas K^+ efflux was not required for inflammasome activation in antimycin A-treated human RPE cells. Collectively, our data emphasize that dysfunctional mitochondria regulate the assembly of inflammasome multiprotein complexes in the human RPE cells. The present study associates AIM2 with the pathogenesis of AMD.

1. Introduction

Age-related macular degeneration (AMD) is the most common cause of blindness among aged people living in the developed countries, and the prevalence is increasing due to the aging of populations (Wong et al., 2014; Li et al., 2019). Currently, almost 80% of AMD patients have the dry form of the disease (Velez-Montoya et al., 2014). While there is an effective intravitreal treatment available for slowing down wet AMD, dry AMD is still lacking of any form of therapy (Handa et al., 2019; Velez-Montoya et al., 2014). Finding a suitable treatment is challenging due to our incomplete understanding of the precise mechanisms and timing of cellular events to this multifactorial disease (Handa et al., 2019).

Mitochondrial dysfunctionality and damaged mitochondrial DNA (mtDNA) in the retinal pigment epithelium (RPE) are early hallmarks of AMD (Kaarniranta et al., 2020). Although normal aging elicits mtDNA damage in the RPE (Barreau et al., 1996; Wang et al., 2008), AMD donors have significantly increased levels of mtDNA damage in their RPE cells in comparison to age-matched controls (Karunadharma et al., 2010; Terluk et al., 2015). Mitochondrial DNA damage has been localized to the genes that encode the subunits of the mitochondrial electron transport chain (ETC), which together with ATP synthase, are responsible for most of the cellular energy production (Terluk et al., 2015). In line with that proposal, reduced ATP generation has been found in RPE cells of AMD donors when compared to controls with no AMD (Ferrington et al., 2017; Golestaneh et al., 2017). Due to the high metabolic demand and the constant production of reactive oxidative species (ROS), the outer retina is highly susceptible to oxidative stress (Lefevere et al., 2017). Elevated oxidative stress can damage not only proteins and lipids but also mitochondrial DNA (Fisher and Ferrington, 2018). Oxidative stress

* Corresponding author. Immuno-Ophthalmology, School of Pharmacy, Faculty of Health Sciences, University of Eastern Finland, P.O.Box 1627, FI-70211, Kuopio, Finland.
** Corresponding author.
E-mail addresses: eveliina.korhonen@uef.fi (E. Korhonen), anu.kauppinen@uef.fi (A. Kauppinen).

https://doi.org/10.1016/j.exer.2021.108687
Received 26 October 2020; Received in revised form 30 April 2021; Accepted 29 June 2021
Available online 1 July 2021

can also cause mitochondrial dysfunction and a subsequent impairment of normal cell homeostasis, which further exacerbates the levels of cellular ROS (Lefevere et al., 2017; Terluk et al., 2019).

Inflammasomes are intracellular multiprotein complexes, which become assembled upon exposure to conserved pattern-associated molecular patterns (PAMPs) from infectious agents or damage-associated molecular patterns (DAMPs) that are alarming signals of cellular distress (Zheng et al., 2020). Depending on the inflammasome, recognition of PAMPs and DAMPs can evoke either direct ligand-binding or act through an indirect mechanism to trigger changes in cellular homeostasis (Christgen et al., 2020). The inflammasome complex typically consists of a receptor, an adaptor protein apoptosis-associated speck-like protein containing a caspase-activation and recruitment domain (ASC), and pro-caspase-1 proteins (Christgen et al., 2020; Malik and Kanneganti, 2017). The formation of the inflammasome complex results in the cleavage of pro-caspase-1, which thereafter proteolytically cleaves immature forms of IL-1β and IL-18 into their biologically active forms (Malik and Kanneganti, 2017). Additionally, caspase-1 activation leads to the cleavage and the oligomerization of gasdermin D, which subsequently forms plasma membrane pores to permit the secretion of IL-1β and IL-18 (Orning et al., 2019).

Thus far, NLRP3 has been the best-characterized inflammasome and its activation has also been implicated in the pathogenesis of AMD (Kauppinen et al., 2016). Previous studies have shown that mitochondrial ROS (Zhou et al., 2010b; Heid et al., 2013; Nakahira et al., 2011) and cytosolic oxidized mtDNA (Shimada et al., 2012) are able to induce NLRP3 inflammasome activation in bone marrow-derived macrophages (BMDMs) (Heid et al., 2013; Shimada et al., 2012; Zhou et al., 2010b; Nakahira et al., 2011) and a human THP-1 macrophage cell line (Zhou et al., 2010b). Absent in melanoma 2 (AIM2) is an inflammasome receptor specialized in recognizing cytosolic DNA fragments (Hornung et al., 2009; Fernandes-Alnemri et al., 2009). Mitochondrial DNA has been shown to induce the activation of the AIM2 inflammasome in BMDMs (Bae et al., 2019; Shimada et al., 2012) and in human keratinocytes (Dombrowski et al., 2012). It has also been shown to induce cyclic GMP-AMP synthase (cGAS)-dependent interferon signaling, which resulted in non-canonical inflammasome activation and secretion of IL-18 in *Alu* RNA-driven retinal degeneration in mice (Kerur et al., 2018). In another study, transfected mtDNA weakly activated caspase-1 and IL-1β in ARPE-19 cells (Dib et al., 2015), suggesting that cytosolic mtDNA may play a role in inflammasome activation in human RPE cells. In order to clarify the complex mechanisms behind the pathobiology of AMD, we investigated whether the inhibition of the mitochondrial ETC complex III by antimycin A would affect the activation of inflammasomes in human RPE cells.

2. Materials and methods

2.1. Cell stimulations

The human retinal pigment epithelial cell line ARPE-19 was purchased from the American Type Culture Collection (ATCC). Cells were cultured in complete DMEM/F12 (1:1) growth medium (Life Technologies, Paisley, UK) containing 10% inactivated fetal bovine serum (FBS; Hyclone, Logan, UT, USA), 2 mM L-glutamine (Lonza, Walkersville, USA), 100 U/ml penicillin (Lonza), and 100 μg/ml streptomycin (Lonza) at +37 °C in humidified conditions with 5% CO_2. Passages 26–36 were used in this study. In the experiments, ARPE-19 cells were seeded onto 12-well plates at a density of 2×10^5 cells per well in the complete growth medium.

Differentiated ARPE-19 cells were cultured on Matrigel-coated (Corning, Corning, NY, USA) 24-well hanging cell culture inserts (Millipore, Burlington, MA, USA) in complete DMEM/F12 growth medium. 0.75×10^5 cells were seeded onto the inserts and maintained for 4 weeks with medium changes every other day.

The human retinal pigment epithelial cells, D407, were maintained in DMEM growth medium (Life Technologies) containing 5% inactivated fetal bovine serum (Hyclone), 2 mM L-glutamine (Lonza), 100 U/ml penicillin (Lonza), and 100 μg/ml streptomycin (Lonza) at +37 °C in humidified conditions with 5% CO_2. Passages 47–49 were used in this study. Cells were routinely passaged twice per week. For experiments, D407 cells were seeded onto 24-well plates at a density of 2×10^5 cells per well in the complete growth medium.

Human embryonal stem cell (hESC)-derived RPE cells were generated as previously described at BioMediTech, Tampere University (Vaajasaari et al., 2011). The use of human embryos for research purposes at BioMediTech has been approved by the National Authority for Medicolegal Affairs Finland (Dnro 1426/32/300/05). The institute also has supportive statements from the Ethical Committee of the Pirkanmaa Hospital District to derive, culture, and differentiate hESC lines (Skottman/R05116). No new cell lines were derived for this study. For experiments hESC-RPE cells were plated on Matrigel-coated (Corning, Corning, NY, USA) 24-well hanging cell culture inserts (Millipore, Burlington, MA, USA) at a density of 7.5×10^4 cells per insert. Cells were maintained in KO-DMEM medium (Life Technologies), supplemented with 15% KO-Serum Replacement (Life Technologies), 1% GlutaMAX (Life Technologies), 1% non-essential amino acids (Lonza), 50 U/ml penicillin (Life Technologies), and 50 μg/ml streptomycin (Life Technologies), as well as 100 μM 2-mercaptoethanol (Life Technologies). Medium above and below the inserts was exchanged every two to three days and cells were maintained in culture for at least 8 weeks prior to experiments until they had formed a dense, highly-pigmented monolayer.

Confluent ARPE-19 and D407 cell layers and differentiated ARPE-19 cells were washed and replaced with serum-free medium containing 2 mM L-glutamine, 100 U/ml penicillin and 100 μg/ml streptomycin. ARPE-19 cells were treated with recombinant human interleukin 1α (IL-1α, 4 ng/ml; R&D Systems, Minneapolis, MN, USA) for 48 h with or without potassium chloride (KCl, 50 mM, Merck, Damstadt, Germany) whereas D407 cells were only treated with IL-1α (4 ng/ml) for 24 h at +37 °C in humidified conditions with 5% CO_2. Thereafter, antimycin A (12.5 μM–50 μM; Sigma, batch no 096M4022V) was added to wells, and the cells were incubated for 1–24 h at +37 °C in humidified conditions with 5% CO_2. Instead, hESC-RPE monolayers were washed with complete culture medium, before being stimulated with 4 ng/ml IL-1α (R&D Systems) in complete culture medium added to both the apical and basal side. After an incubation for 48 h, cells were exposed to antimycin A (100–400 μM, Sigma) from both the apical and basal side.

ARPE-19 cells were additionally treated with caspase-1 inhibitor (Ac-YVAD-CMK, 50 μM; Calbiochem, Millipore, Billerica, MA, USA), ammonium pyrrolidinedithiocarbamate (APDC, 50 μM; Sigma), mito-TEMPO (50 μM; Enzo, Farmingdale, NY, USA), diphenyleneiodonium chloride (DPI, 10–30 μM; Sigma), glyburide (50–200 μM; Sigma), or MCC950 (50 μM; Cayman Chemicals) for 1 h or alternatively with bafilomycin A (50 nM; Sigma) for 24 h prior to antimycin A treatment. All the cell culture medium samples and cell lysates were collected 1–24 h following the antimycin A treatment as previously described (Korhonen et al., 2019). Protein concentrations from cell lysates were measured using the Bradford method (Bradford, 1976). Additionally, medium samples from the apical and basal side of the hESC-RPE cells were collected separately, centrifuged at $380 \times g$ for 10 min, and the supernatants were used for further analysis.

In the present study, MG-132 + bafilomycin A and Poly(dA:dT)-treated ARPE-19 cells served as positive controls for NLRP3 and AIM2 inflammasome activations, respectively (Piippo et al., 2014; Hornung et al., 2009). For NLRP3 activation, ARPE-19 cells were primed with IL-1α for 24 h and then exposed to MG-132 (5 μM; Calbiochem, San Diego, CA, USA) for the next 24 h and to bafilomycin A (50 nM) for additional 24 h before the sample collection, which has been described previously (Korhonen et al., 2019). For AIM2 activation, Poly(dA:dT) (0.5 μg/ml; Merck) transfections were performed 48 h after the IL-1α treatment using Lipofectamine 2000 (Thermo) transfection reagent in

Opti-MEM medium (Gibco) according to the manufacturers' instructions. Thereafter, ARPE-19 cells were incubated for 24 h. Where applicable, ARPE-19 cells were treated with the specific NLRP3 inhibitor MCC950 (50 μM) either concurrently with MG-132 or 1 h prior to the poly(dA:dT) treatment.

2.2. Enzyme-linked immunosorbent assay (ELISA)

Human IL-1β (BD Bioscience, San Diego, CA, USA), IL-18 (eBioscience, San Diego, CA, USA), and NLRP3 (Cusabio, Wuhan, China) were measured from cell culture medium samples using the ELISA method according to the manufacturer's instructions. Additionally, pro-IL-1β was detected from cell culture medium samples and cell lysates following the manufacturer's instructions (R&D, Minneapolis, MN, USA). Equal amounts of protein from each cell lysate sample were used in the assay of pro-IL-1β. Absorbance values from all ELISA assays were measured using a spectrophotometer (Biorad, Model 550, Hercules, CA, USA) at the wavelength of 450 nm with the reference wavelength of 655 nm.

2.3. Lactate dehydrogenase (LDH) assay

LDH was measured from cell culture medium samples using the commercial CytoTox96® Non-Radioactive Cytotoxicity assay (Promega, Madison, WI, USA) according to the manufacturer's protocol. Absorbances after the colorimetric reaction were measured using a spectrophotometer (Cytation 3, Biotek Instruments, Inc. Winooski, VT, USA) at the wavelength of 490 nm.

2.4. 2′,7′-dichlorodihydrofluorescein diacetate (H_2DCFDA) assay

ARPE-19 cells were seeded onto 96-well plates at a density of 1.5×10^4 cells per well in the complete growth medium, which was replaced by serum-free medium at the beginning of exposures. Confluent cell cultures were treated with IL-1α (4 ng/ml) as described above. In the measurement of intracellular ROS, cells were treated with APDC (50–100 μM) for 1 h prior to the addition of cell permeable H_2DCFDA (5 μM; Invitrogen, Eugene, OR, USA) and antimycin A (25 μM). Thereafter, the cells were incubated for 1 h at +37 °C in humidified conditions with 5% CO_2 and washed twice with 1 × phosphate buffered saline (PBS). The fluorescence signal was immediately detected using a fluorometer (Cytation 3, Biotek Instruments, Inc. Winooski, VT, USA) at the excitation and emission wavelengths of 488 nm and 528 nm, respectively. Cells without the H_2DCFDA probe were used as negative controls with their values being subtracted from the results of cells exposed to H_2DCFDA.

2.5. ROS-Glo assay

The production of H_2O_2 was measured using the commercial Ros-Glo assay (Promega, Madison, WI, USA). In the analysis, ARPE-19 cells were seeded onto 96-well plates with white walls and clear bottoms (Greiner) at the density of 2×10^4 cells and incubated for 48 h at +37 °C in humidified conditions with 5% CO_2. Cells were primed with IL-1α (4 ng/ml) as described above. The ROS-Glo assay substrate (25 μM) was added along with antimycin A (25 μM). After a 1 h incubation, detection solution was added and the plates were incubated at room temperature (RT) for 20 min. Thereafter, the luminescent signal was detected using a luminometer (Cytation 3). H_2O_2-treated (1 mM; Sigma) ARPE-19 cells served as the positive control.

2.6. NLRP3 and AIM2 knockdown

For the siRNA experiments ARPE-19 cells were seeded onto 12-well plates at a density of 1.5×10^5 cells per well whereas D407 cells were seeded onto 48-well plates at a density of 8×10^4 cells per well. Subconfluent (60–80%) cell cultures were washed and replaced with fresh medium without antibiotics, and the cells were further treated with the Silencer Select NLRP3 siRNA (ID: s41556; Ambion by Life Technologies) or Silencer Select AIM2 siRNAs (IDs: s18092 and s18094; Ambion) with Lipofectamine® RNAiMAX Reagent (Invitrogen, Van Allen Way Carlsbad, CA, USA) according to the manufacturer's instructions and our previous studies (Piippo et al., 2014; Korhonen et al., 2020). Mixtures of siRNAs with the transporter were prepared in the Opti-MEM medium (Gibco, Grand Island, NY, USA). ARPE-19 and D407 cells were incubated for 24 h at +37 °C in humidified conditions with 5% CO_2 and fresh serum-free medium was changed along with the addition of the priming factor IL-1α. Thereafter, cell cultures were incubated for another 24 h at +37 °C in humidified conditions with 5% CO_2. Antimycin A exposure was performed as described above. Silencer select Negative control siRNA (Ambion) was used as a negative control.

2.7. Immunofluorescence staining

ARPE-19 cells were cultured on coverslips in 24-well plates (Costar) at a density of 1×10^5 cells per well in the complete growth medium and incubated for 48 h at +37 °C in humidified conditions with 5% CO_2. IL-1α (4 ng/ml) and antimycin A (25 μM) treatments were performed as described above. After 6 h of antimycin A exposure, ARPE-19 cells were washed twice with PBS and fixed by 4% paraformaldehyde (PFA) for 15 min at RT. Thereafter, the cells were washed three times in PBS and permeabilized with 0.1% Triton X-100 (Sigma) in PBS for 15 min at RT following the blocking with 3% BSA in PBS for 1h at RT. p22-phox was detected using mouse monoclonal p22-phox antibody (cas. nro. sc-271 262; 1:500 in 3% BSA in PBS; Santa Cruz) overnight at +4 °C. This antibody has previously been used with ARPE-19 cells (Qiu et al., 2015). Thereafter, the cells on the coverslips were washed three times for 5 min with 1 × PBS followed by a 2 h incubation at RT with goat anti-rabbit IgG secondary Alexa Fluor 594 antibody (1:1000; in 3% BSA in PBS; ThermoFischer). After washing three times for 5 min in 1 × PBS, the samples were counterstained with 4′, 6-diamidino-2-phenylindole dihydrochloride (DAPI; 1:10 000 in PBS; Sigma) prior to mounting of the cells on coverslips with Mowiol (Sigma). Images were viewed under an immunofluorescence microscope (Zeiss) and analyzed using the ImageJ program. Background fluorescence was subtracted using the following formula: corrected total cell fluorescence (CTCF) = integrated density – (area of selected cell × mean fluorescence of background).

2.8. FLICA staining

ARPE-19 cells were seeded onto 8-well chamber slides with removable wells (Nunc Lab-Tek II Chamber Slide) at a density of 4×10^4 cells per well in a complete growth medium and incubated for 48 h at +37 °C in humidified conditions with 5% CO_2. Moreover, D407 cells were seeded onto 8-well chamber slides with removable wells (Nunc Lab-Tek II Chamber Slide) at a density of 1×10^5 cells per well in complete growth medium and incubated for 72 h at +37 °C in humidified conditions with 5% CO_2. Thereafter, ARPE-19 and D407 cells were washed once and medium was replaced with serum-free medium containing IL-1α (4 ng/ml) and incubated for 48 h and 24 h prior to antimycin A exposure, respectively. FLICA reagent, FAM-YVAD-FMK (1:300, ImmunoChemistry Technologies, Bloomington, MN, USA) was loaded onto the cells at 5 h after the addition of antimycin A and the cells were incubated for an additional 1 h at +37 °C in humidified conditions with 5% CO_2. Thereafter, cells were washed three times with a commercial washing buffer provided by the manufacturer prior to counterstaining with Hoechst33342 (Invivogen) for 15 min at +37 °C. Stained cells were fixed by 4% PFA for 15 min at RT. Thereafter, cells were washed with 1 × DPBS. Polystyrene media chambers were removed from the glass slide and the mounting medium was used to immobilize coverslip over the specimen. Samples were observed under the fluorescence microscope (Zeiss) using excitation and emission wavelengths of 492 nm and 520

nm for FLICA and excitation and emission wavelengths of 360 nm and 460 nm for Hoechst33342, respectively.

2.9. Microscale thermophoresis

Microscale thermophoresis (MST) was used to determine antimycin A binding to melanin as described earlier (Hellinen et al., 2020). Soluble melanin microparticles were prepared from synthetic melanin (Sigma) as previously described (Hellinen et al., 2020). The solution of 10 mg/ml melanin microparticles (in PBS) was mixed with the solution of 200 μM antimycin A (in PBS containing 4% ethanol and 16% DMSO) or with solvent only and incubated for 1 h at room temperature, protected from light. Low-binding pipette tips (Corning Incorporated, Salt Lake City, USA) and tubes (Alpha Laboratories, Hampshire, UK) were used for all handling steps. After 1 h, the melanin-antimycin A complexes (final concentration 200 μM antimycin A, 5 mg/ml melanin) were mixed gently before being loaded into capillaries (NanoTemper Technologies GmbH, Germany). The samples were analyzed with a Monolith NT.115 pico device using MO.Control Software (both from NanoTemper Technologies GmbH) using nano-blue excitation, LED light adjusted to 80% excitation power, and infrared laser power set to high.

2.10. Statistical analysis

Statistical analysis was performed using the GraphPad Prism software (GraphPad Software, San Diego, CA, USA version 8.1.2). Pairwise comparisons were performed using the Mann-Whitney *U* test. *P*-values of 0.05 or less were considered as statistically significant.

3. Results

3.1. Antimycin A-induced mitochondrial damage results in the production of mature IL-1β

To investigate whether mitochondrial damage induces inflammasome activation in ARPE-19 cells, the cells were first primed with IL-1α. A priming signal is required to induce the expression of inflammasome components pro-IL-1β and NLRP3 in RPE cells (Korhonen et al., 2020; Piippo et al., 2018b). Thereafter, ARPE-19 cells were exposed to the mitochondrial electron transport chain (ETC) complex III inhibitor,

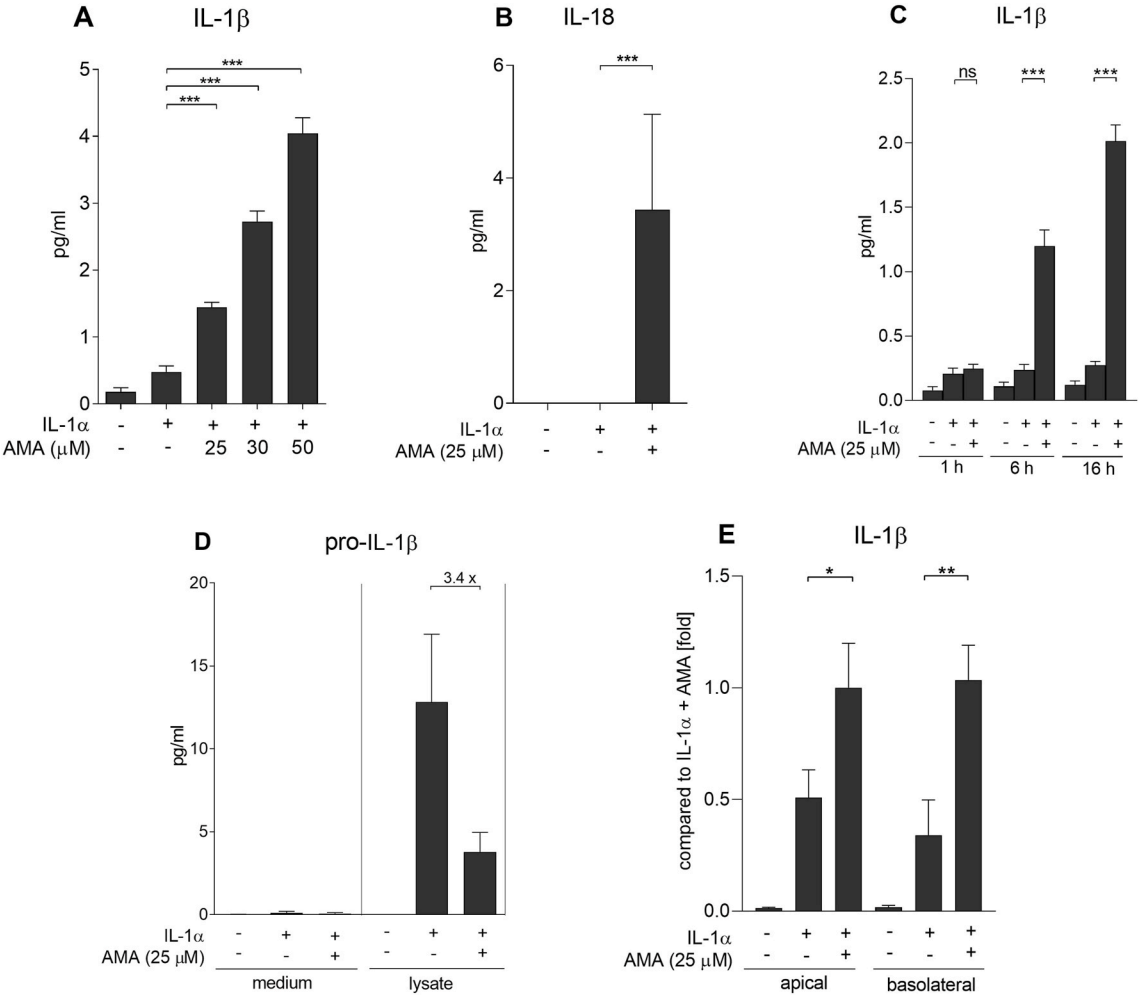

Fig. 1. Antimycin A induces the secretion of IL-18 as well as time and dose-dependent production of mature IL-1β in human RPE cells. ARPE-19 cells were primed with IL-1α (4 ng/ml) for 48 h and exposed to antimycin A. IL-1β was measured using the ELISA method from cell culture medium samples 24 h after addition of antimycin A (25–50 μM) (A). Alternatively, extracellular IL-18 was measured after ARPE-19 cells were exposed to antimycin A (25 μM) for 24 h (B). IL-1β secretion was also detected at 1 h, 6 h, and 16 h after the antimycin A (25 μM) exposure (C). Pro-IL-1β was measured using the ELISA from cell culture medium and cell lysate samples after ARPE-19 cells were exposed to antimycin A (25 μM) for 24 h (D). Similar settings were also used when IL-1β was determined from cell culture medium samples collected from apical and basolateral sides of differentiated ARPE-19 cells (E). The data on undifferentiated ARPE-19 cells were combined from three independent experiments with 3–4 parallel samples in each group, except the data on IL-18, which was combined from four independent experiments using four parallel samples in each group. The data on differentiated ARPE-19 cells were combined from four independent experiments with 2–3 parallels in each group. All data (A–E) are presented as mean ± SEM and analyzed using Mann-Whitney *U* test. $^{*)}$ $p < 0.05$, $^{**)}$ $p < 0.01$, $^{***)}$ $p < 0.001$, $^{ns)}$ not significant. AMA = antimycin A.

antimycin A (25–50 μM). The secretion of IL-1β was dose-dependently increased 24 h after the antimycin A treatment in IL-1α-primed ARPE-19 cells (Fig. 1 A; mean ± SEM for IL-1α: 0.48 ± 0.09 pg/ml, IL-1α + 25 μM antimycin A: 1.44 ± 0.08 pg/ml, IL-1α + 30 μM antimycin A: 2.73 ± 0.16 pg/ml, and IL-1α + 50 μM antimycin A: 4.04 ± 0.23 pg/ml; all $p < 0.001$). Since 25 μM of antimycin A was sufficient to induce a significant production of IL-1β in ARPE-19 cells, this concentration was used in subsequent experiments. In line with the secretion of IL-1β, antimycin A (25 μM) was found to induce the secretion of IL-18 in IL-1α-primed ARPE-19 cells when IL-18 was measured 24 h after antimycin A exposure (Fig. 1 B; mean ± SEM for IL-1α: 0 pg/ml and IL-1α + antimycin A: 3.44 ± 1.69 pg/ml; $p < 0.01$). Antimycin A (25 μM) did not induce the production of IL-1β 1 h after the exposure but IL-1β levels were statistically significantly increased at the 6 h time point (Fig. 1 C; mean ± SEM for IL-1α: 0.24 ± 0.04 pg/ml and IL-1α + antimycin A: 1.20 ± 0.13 pg/ml; $p < 0.001$), and further elevated time-dependently by the 16 h time point (Fig. 1 C; mean ± SEM for IL-1α: 0.27 ± 0.03 pg/ml and IL-1α + antimycin A: 2.01 ± 0.13 pg/ml; $p < 0.001$).

Next, we verified that antimycin A-induced IL-1β was the mature cytokine instead of passively leaked pro-IL-1β. As expected, priming with IL-1α induced the production of intracellular pro-IL-1β (Fig. 1 D; mean ± SEM for untreated control: 0 pg/ml; IL-1α: 12.84 ± 4.08 pg/ml).

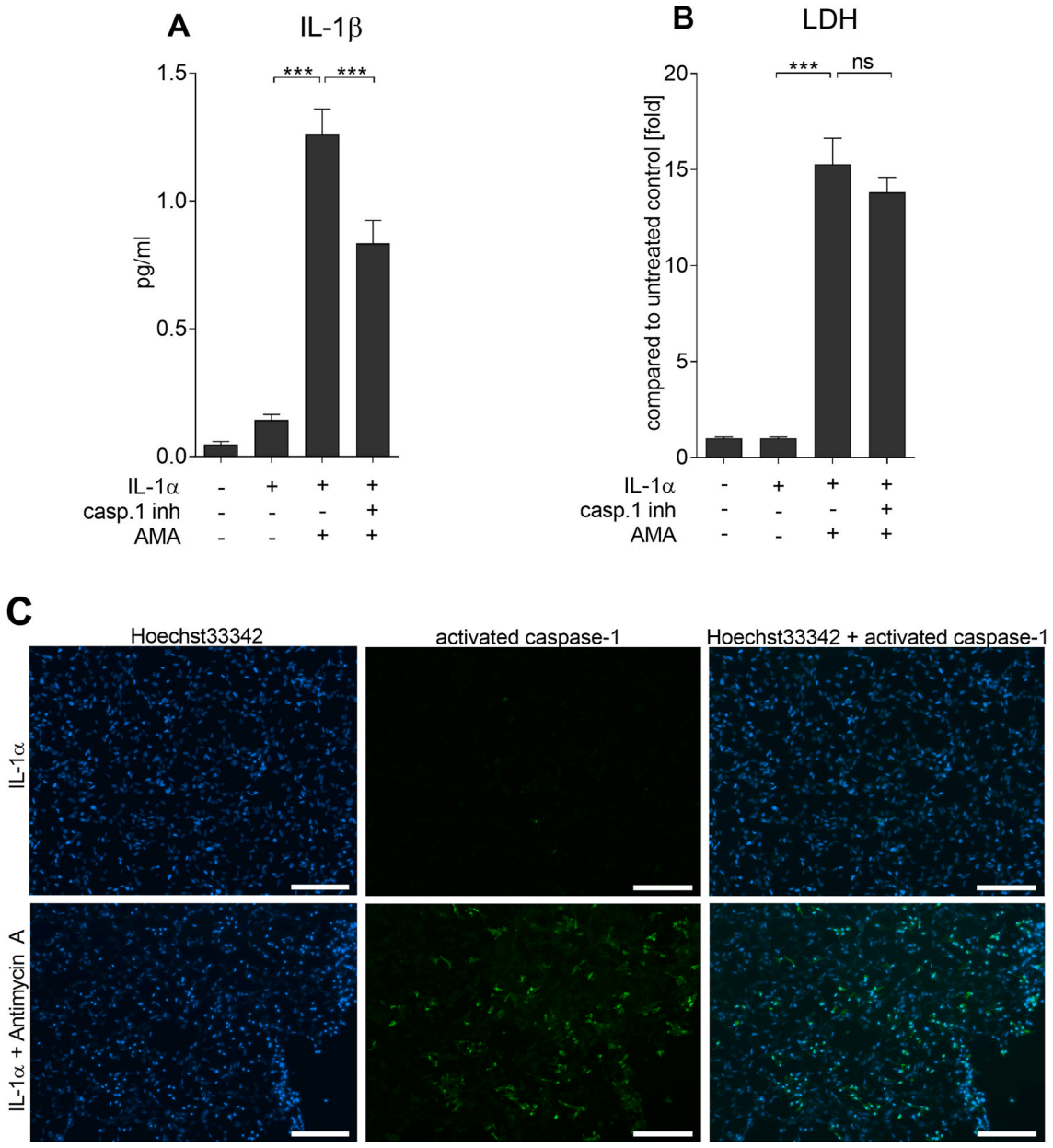

Fig. 2. Antimycin A induces the activation of caspase-1 in ARPE-19 cells. ARPE-19 cells were primed with IL-1α (4 ng/ml) for 24 h and exposed to antimycin A (25 μM) for the subsequent 24 h. Caspase-1 inhibitor (50 μM) was added 1 h prior to the antimycin A exposure. IL-1β was measured using the ELISA method (A) and LDH leakage using a commercial cytotoxicity assay (B). Data from IL-1β measurements were combined from four independent experiments with 6 parallels of untreated control and IL-1α-treated cells and 6 or 12 parallels of IL-1α + antimycin A and IL-1α + caspase-1 inhibitor + antimycin A-treated cells. Data from LDH experiments were combined from three independent experiments with 6 parallel samples in each group. Activation of caspase-1 was detected using the FLICA probe FAM-YVAD-FMK under the fluorescence microscope 6 h after the antimycin A treatment (C). Panels from left to right are showing nucleus (blue), activated caspase-1 (green), and merged image (C). The FLICA assay was repeated three times and different treatment groups were photographed using the identical microscope settings with 10-fold objective (scale bar, 100 μm). Data (A–B) are presented as mean ± SEM and analyzed using Mann-Whitney *U* test. ***) p < 0.001, ns) not significant. casp. 1. inh = caspase-1 inhibitor, AMA = antimycin A.

Intracellular pro-IL-1β levels were 3.4-times lower in antimycin A-treated ARPE-19 cells than in primed cells without antimycin A exposure, suggesting that pro-IL-1β had been matured by antimycin A (Fig. 1 D; mean ± SEM for IL-1α: 12.84 ± 4.08 pg/ml and IL-1α + antimycin A: 3.78 ± 1.19 pg/ml). Additionally, pro-IL-1β was absent from antimycin A-treated cell culture medium samples confirming that antimycin A did not cause a leakage of pro-IL-1β from the cell (Fig. 1 D).

In addition to experiments with undifferentiated ARPE-19 cells, the antimycin A-induced production of IL-1β was measured from both apical and basolateral sides of differentiated ARPE-19 cells. Antimycin A (25 μM) significantly increased the production of mature IL-1β on both sides when compared to cells not exposed to antimycin A (Fig. 1 E; mean ±

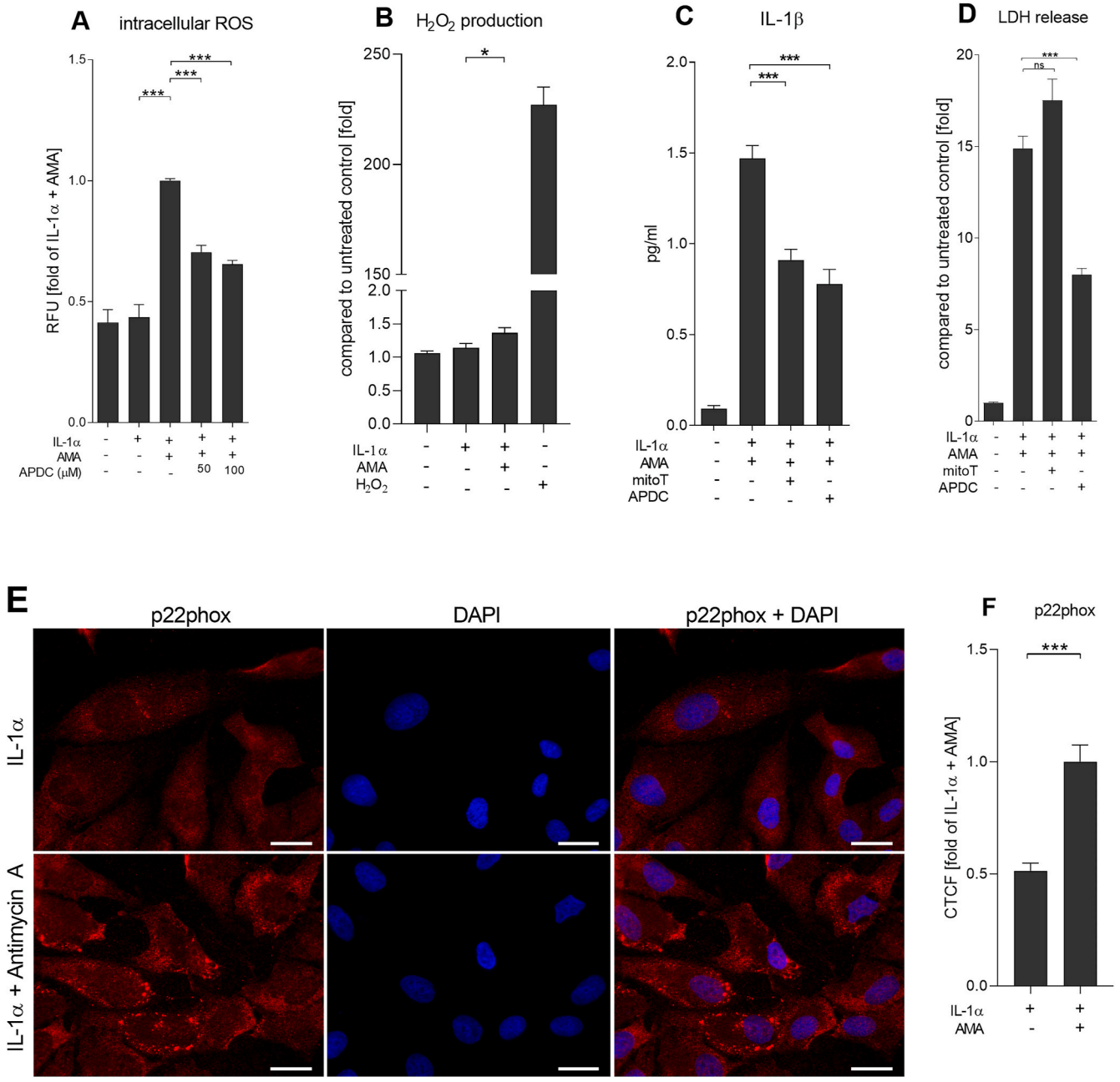

Fig. 3. Antimycin A induces mitochondrial and NADPH oxidase-dependent ROS production, which results in IL-1β secretion in ARPE-19 cells. ARPE-19 cells were primed with IL-1α (4 ng/ml) and exposed to antimycin A (25 μM) for 24 h. Intracellular ROS was measured using H_2DCFDA assay 1 h after the antimycin A exposure (A). APDC (50–100 μM) was added 1 h prior to the antimycin A exposure where applicable. Data from H_2DCFDA assay were combined from three independent experiments with six parallel samples in each group. The production of H_2O_2 was measured 1 h after the antimycin A exposure using the ROS-Glo assay (B). Data from the ROS-Glo assay were combined from three independent experiments with four parallel samples in each group. The production of IL-1β was measured 24 h after the antimycin A exposure using the ELISA method from cell culture medium samples (C). Moreover, LDH leakage was detected using a commercial cytotoxicity assay (D). MitoTEMPO (50 μM) or APDC (50 μM) were added 1 h prior to the antimycin A exposure where applicable (C–D). Data of IL-1β and LDH were combined from three independent experiments with six parallel samples in each group. Immunofluorescence staining of p22phox was performed 6 h after the antimycin A exposure (E–F). Immunofluorescence stainings were repeated three times and different treatment groups were photographed with similar settings using a 40-fold objective (scale bar, 20 μm). Representative images from left to right panels are presenting p22phox (red), nucleus (blue), and merged image (E). Fluorescence images were quantified counting 50 cells (F). All data (A–E) are presented as mean ± SEM and analyzed using Mann-Whitney *U* test. $^{*)}$ $p < 0.05$, $^{**)}$ $p < 0.01$, $^{***)}$ $p < 0.001$, $^{ns)}$ not significant. mitoT = mitoTempo, AMA = antimycin A, RFU = relative fluorescent unit, CTCF = corrected total cell fluorescence.

SEM in apical side for IL-1α: 22.97 ± 6.12 pg/ml and IL-1α + antimycin A: 49.05 ± 13.95 pg/ml, $p < 0.05$; mean ± SEM in basolateral side for IL-1α: 0.71 ± 0.17 pg/ml and IL-1α + antimycin A: 4.28 ± 1.15 pg/ml, $p < 0.01$). Thereafter, antimycin A-induced production of IL-1β and IL-18 were confirmed using another RPE cell line, D407. We found that antimycin A dose-dependently increased the secretion of IL-1β (Suppl. Fig. 1 A: mean ± SEM for IL-1α: 2.1 ± 0.09 pg/ml, IL-1α + 12.5 μM antimycin A: 8.7 ± 0.22 pg/ml, IL-1α + 25 μM antimycin A: 10.5 ± 0.33 pg/ml, and IL-1α + 50 μM antimycin A: 18.7 ± 0.66 pg/ml; all $p < 0.001$) and IL-18 (Suppl. Fig. 1 B: mean ± SEM for IL-1α: 12.0 ± 0.75 pg/ml, IL-1α + 12.5 μM antimycin A: 61.4 ± 4.1 pg/ml, IL-1α + 25 μM antimycin A: 104.8 ± 5.4 pg/ml, and IL-1α + 50 μM antimycin A: 278.9 ± 11.46 pg/ml; all $p < 0.001$) in IL-1α-primed D407 cells. These results together confirm that antimycin A-induced mitochondrial damage results in the activation of IL-1β and IL-18 in human RPE cells. All subsequent experiments have been performed using non-pigmented ARPE-19 and D407 cells since we found that antimycin A binds to melanin (Suppl. Fig. 1 C, $p < 0.0001$). Despite high antimycin A concentrations (100–400 μM), LDH leakage (Suppl. Fig. 1 D) and the secretion of IL-1β (Suppl. Fig. 1 E) from highly-pigmented hESC-RPE cells remained low.

3.2. Antimycin A-induced production of IL-1β is dependent on caspase-1 activation

In order to study whether IL-1β release was regulated by the inflammasome, we added an irreversible inhibitor of caspase-1 to the cell cultures prior to the inflammasome activation. As shown in Fig. 2A, antimycin A-induced production of IL-1β was significantly reduced by the caspase-1 inhibitor (mean ± SEM for IL-1α + antimycin A: 1.26 ± 0.10 pg/ml and IL-1α + caspase-1 inhibitor + antimycin A: 0.83 ± 0.09 pg/ml; $p < 0.001$). The unchanged levels of LDH indicate that the reduced IL-1β levels did not result from the cytotoxicity of the inhibitor (Fig. 2 B; $p > 0.05$). The regulation of the inflammasome activation by caspase-1 was confirmed using the FLICA assay, which displayed an increased fluorescence of the caspase-1-targeted probe in the antimycin A-treated ARPE-19 cells (Fig. 2 C) and D407 cells (Suppl. Fig. 2) when compared to cells without antimycin A. Our results demonstrated that mitochondrial damage leads to inflammasome activation, which is dependent on caspase-1 activation in RPE cells.

3.3. Antimycin A-induced secretion of IL-1β is dependent on mitochondrial and NADPH oxidase-mediated ROS production

It has been proposed that ROS production is one major mechanism of NLRP3 inflammasome activation (Zhou et al., 2010a). Therefore, we investigated whether the inhibition of mitochondrial electron transport chain complex III by antimycin A could induce the production of ROS upstream of the inflammasome activation in ARPE-19 cells. First, intracellular levels of ROS were detected using the H_2DCFDA assay. Data showed that mitochondrial damage significantly increased the levels of intracellular ROS in ARPE-19 cells already at 1 h after the antimycin A treatment (Fig. 3 A; $p < 0.001$). Antimycin A significantly increased also the production of H_2O_2 (Fig. 3 B; $p < 0.05$). The ROS scavenger APDC reduced the ROS levels (Fig. 3 A; $p < 0.001$) and the production of IL-1β (Fig. 3 C; mean ± SEM for IL-1α + antimycin A: 1.47 ± 0.07 pg/ml and IL-1α + APDC + antimycin A: 0.78 ± 0.08 pg/ml; $p < 0.001$) in antimycin A-treated ARPE-19 cells when compared to cells without APDC. In line with that, the mitochondrial ROS scavenger mito-TEMPO reduced antimycin A-induced secretion of IL-1β (Fig. 3 C; mean ± SEM for IL-1α + antimycin A: 1.47 ± 0.07 pg/ml and IL-1α + mito--TEMPO + antimycin A: 0.91 ± 0.06 pg/ml; $p < 0.001$). Mito-TEMPO was not cytotoxic, and APDC even diminished the release of LDH from antimycin A-treated ARPE-19 cells (Fig. 3 D). Additionally, DPI, a well characterized NADPH oxidase inhibitor (Augsburger et al., 2019), reduced the production of IL-1β (Suppl. Fig. 3 A; mean ± SEM for IL-1α + antimycin A: 2.20 ± 0.28 pg/ml, IL-1α + DPI 10 μM + antimycin A: 1.63 ± 0.27 pg/ml, IL-1α + DPI 20 μM + antimycin A: 0.94 ± 0.08 pg/ml, and IL-1α + DPI 30 μM + antimycin A: 0.95 ± 0.05 pg/ml; all $p < 0.001$). However, DPI appeared mildly cytotoxic in ARPE-19 cells (Suppl. Fig. 3 B). The role of NADPH oxidase in antimycin A-exposed ARPE-19 cells was confirmed by the immunofluorescence staining of NADPH oxidase regulator, p22phox. The expression of p22phox was significantly and 1.9-times higher 6 h after the antimycin A treatment when compared to cells without antimycin A (Fig. 3 E-F; $p < 0.001$). In summary, these results demonstrate that antimycin A-induced mitochondrial damage causes mitochondrial and NADPH oxidase-dependent ROS production upstream of the inflammasome activation in ARPE-19 cells.

3.4. Potassium efflux is not involved in the antimycin A-induced inflammasome activation

In addition to the ROS production, K^+ efflux is another major mechanism of NLRP3 inflammasome activation (Pétrilli et al., 2007; Muñoz-Planillo et al., 2013). In order to block the potassium efflux, ARPE-19 cells were exposed to excessive concentrations of extracellular potassium chloride (KCl; 50 mM) prior to the antimycin A stimulation, as previously described (Piippo et al., 2018a; Korhonen et al., 2020). Surprisingly, excessive extracellular KCl preferably increased rather than decreased the production of IL-1β in ARPE-19 cells upon the antimycin A treatment (Fig. 4 A; mean ± SEM for IL-1α + antimycin A: 1.20 ± 0.15 pg/ml and IL-1α + KCl + antimycin A: 1.55 ± 0.12 pg/ml; $p < 0.001$). The result was verified by treating ARPE-19 cells with the potassium channel inhibitor, glyburide. Similarly to the excessive potassium, glyburide significantly increased the secretion of IL-1β (Fig. 4 B; mean ± SEM for IL-1α + antimycin A: 1.58 ± 0.08 pg/ml and IL-1α + glyburide 50 μM + antimycin A: 1.88 ± 0.08 pg/ml; $p < 0.05$). The glyburide-induced production of IL-1β in antimycin A-exposed ARPE-19 cells was dose-dependent (Suppl. Fig. 4).

3.5. AIM2 and NLRP3 inflammasomes are involved in antimycin A-induced production of IL-1β in human RPE cells

Finally, we evaluated the responsible inflammasome receptor in antimycin A-induced IL-1β maturation. Surprisingly, it was found that NLRP3 knockdown preferentially increased rather than decreased the production of IL-1β when compared to the non-specific siRNA in ARPE-19 cells (Fig. 5 A; mean ± SEM for non-specific siRNA + IL-1α + antimycin A: 6.66 ± 0.18 pg/ml and NLRP3 siRNA + IL-1α + antimycin A: 9.09 ± 0.40 pg/ml, $p < 0.01$). Correspondingly, NLRP3 knockdown mildly increased the secretion of IL-18 when compared to non-specific siRNA -transfected ARPE-19 cells, but the difference was not statistically significant (Suppl. Fig. 5 A; mean ± SEM for non-specific siRNA + IL-1α + antimycin A: 18.30 ± 3.55 pg/ml and NLRP3 siRNA + IL-1α + antimycin A 19.78 ± 4.53 pg/ml; $p > 0.05$). As NLRP3 has previously been shown to be either secreted out from the cell or degraded by autophagy after the inflammasome activation (Piippo et al., 2018b), the extracellular level of NLRP3 was measured. Antimycin A slightly reduced the extracellular NLRP3 (Fig. 5 B; mean ± SEM for IL-1α: 1035.67 ± 48.09 ng/ml and IL-1α + antimycin A: 836.58 ± 41.84 ng/ml; $p < 0.01$). Additionally, the levels of extracellular NLRP3 were measured upon blocking the autophagy by bafilomycin A. This treatment had no effect on the secretion of NLRP3 (Fig. 5 B; mean ± SEM for IL-1α + antimycin A: 836.58 ± 41.84 ng/ml and IL-1α+ bafilomycin A + antimycin A: 917.53 ± 51.43 ng/ml, $p > 0.05$). The potential role of NLRP3 was further studied by the selective NLRP3 inhibitor MCC950, which statistically significantly reduced the production of IL-1β in antimycin A-exposed ARPE-19 cells when compared to cells without the inhibitor (Fig. 5 C; mean ± SEM for IL-1α + antimycin A: 1.19 ± 0.09 pg/ml and IL-1α + MCC950 + antimycin A: 0.82 ± 0.08 pg/ml; $p < 0.05$). MCC950 also diminished the production of IL-1β when autophagy and proteasomes were blocked with bafilomycin A and MG-132,

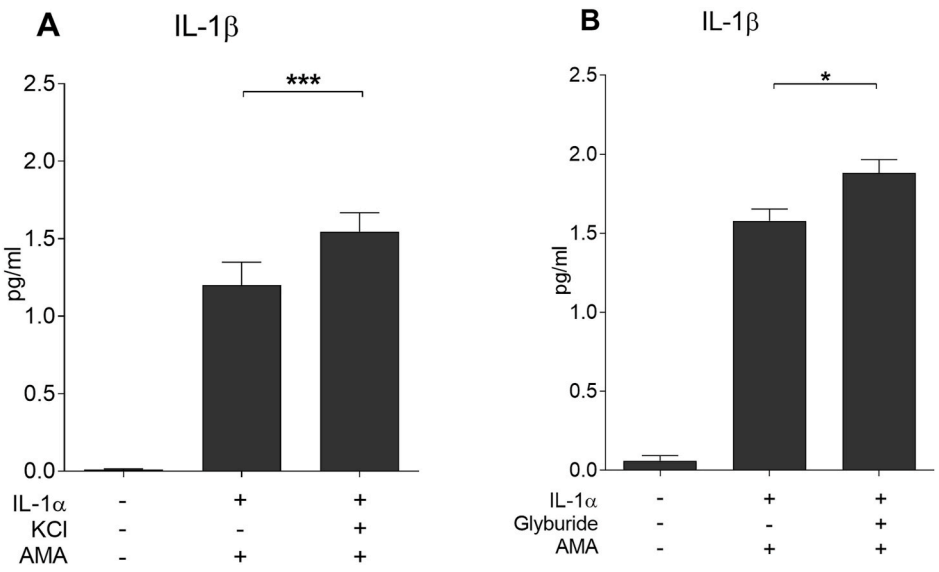

Fig. 4. KCl and glyburide increase antimycin A-induced production of IL-1β in ARPE-19 cells. ARPE-19 cells were primed with IL-1α (4 ng/ml) for 24 h and exposed to antimycin A (25 μM) for the subsequent 24 h. KCl (50 mM) was added along with IL-1α (A) and glyburide (50 μM) 1 h prior to antimycin A exposure (B). IL-1β production was measured by an ELISA method (A–B). Data from KCl experiments were combined from two independent experiments with 5–6 parallel samples of untreated control and IL-1α-treated cells and 5–12 parallel samples of IL-1α + antimycin A and IL-1α + KCl + antimycin A-treated cells. Data from glyburide experiments were combined from two independent experiments with 4–6 parallel samples in each group. All data (A–B) are presented as mean ± SEM and analyzed using Mann-Whitney *U* test. *) $p < 0.05$, ***) $p < 0.001$. AMA = antimycin A.

respectively (Fig. 5 C; mean ± SEM for IL-1α + MG-132 + bafilomycin A: 3.71 ± 0.13 pg/ml and IL-1α + MCC950 + MG-132 + bafilomycin A: 2.98 ± 0.15 pg/ml; $p < 0.01$) but it had no alleviating effect on the production of IL-1β when ARPE-19 cells were exposed to poly(dA:dT) (Fig. 5 C; mean ± SEM for IL-1α + poly(dA:dT): 2.26 ± 0.07 pg/ml and IL-1α + MCC950 + poly(dA:dT): 3.11 ± 0.16 pg/ml; $p < 0.001$). The concentration of MCC950 used in this study was not cytotoxic in ARPE-19 cells (Suppl. Fig. 5 B).

In contrast to the NLRP3 siRNA, knockdown of AIM2 significantly reduced the antimycin A-induced production of IL-1β when compared to the non-specific siRNA (Fig. 5 D; mean ± SEM for non-specific siRNA + IL-1α + antimycin A: 3.55 ± 0.19 pg/ml, AIM2 siRNA s18092 + IL-1α + antimycin A: 0.66 ± 0.05 pg/ml, and AIM2 siRNA s18094 + IL-1α + antimycin A: 2.33 ± 0.08 pg/ml, both $p < 0.001$). Reduced IL-1β levels were detected using two different AIM2 siRNA constructs and both diminished the production IL-1β in antimycin A-exposed ARPE-19 cells (Fig. 5 D). In line with that, the knockdown of AIM2 reduced the secretion of IL-18, but the difference was not statistically significant (Suppl. Fig. 5 C; mean ± SEM for non-specific siRNA + IL-1α + antimycin A: 1.89 ± 0.51 pg/ml and AIM2 siRNA s18092 + IL-1α + antimycin A: 1.31 ± 0.47 pg/ml; $p > 0.05$). Additionally, LDH was measured 24 h after the AIM2 siRNA knockdown and there were no signs of cell death due to transfections (Suppl. Fig. 5 D).

Lastly, NLRP3 and AIM2 knockdown experiments were repeated on D407 cells, and both NLRP3 siRNA and AIM2 siRNAs reduced the production of IL-1β (Fig. 5 E; mean ± SEM for non-specific siRNA + IL-1α + antimycin A: 12.3 ± 0.65 pg/ml, AIM2 siRNA s18092 + IL-1α + antimycin A: 3.3 ± 0.23 pg/ml, and NLRP3 siRNA + IL-1α + antimycin A: 5.9 ± 0.60 pg/ml). The reduction of IL-1β did not result from cell death (Suppl. Fig. 5 E). Additionally, AIM2 knockdown decreased the production of IL-18 whereas NLRP3 knockdown increased it in D407 cells (Suppl. Fig. 5 F; mean ± SEM for non-specific siRNA + IL-1α + antimycin A: 49.9 ± 3.15 pg/ml, AIM2 siRNA s18092 + IL-1α + antimycin A: 21.0 ± 3.3 pg/ml, and NLRP3 siRNA + IL-1α + antimycin A: 84.2 ± 8.0 pg/ml). Collectively, these results suggest that AIM2 and NLRP3 are both involved in the production of IL-1β in situations of mitochondrial damage induced by antimycin A in human RPE cells. Instead of NLRP3, AIM2 regulates the production of IL-18 in antimycin A-induced RPE cells. As knockdown of AIM2 efficiently blocked the production of IL-1β and IL-18 in both RPE cell lines, these data emphasize the novel role of AIM2 as a crucial inflammasome receptor in human RPE cells upon mitochondrial damage.

4. Discussion

The loss of mitochondrial membrane potential (MMP) results in a failure of ATP production, a disruption of mitochondrial membrane integrity, and causes the release of reactive oxidative species (ROS), mitochondrial DNA (mtDNA), and other mitochondrial components into the cytosol (Banoth and Cassel, 2018). Dysfunctional mitochondria and damaged mtDNA are both closely associated with the pathogenesis of a severe eye disease, age-related macular degeneration (AMD) (Kaarniranta et al., 2020). We have recently shown that the mitochondrial electron transport chain (ETC) complex III inhibitor, antimycin A, dysregulates mitochondrial function, causes a rapid MMP loss, and damages oxidative phosphorylation in human retinal pigment epithelial (RPE) cells (Hytti et al., 2019). In the present study, we demonstrated that antimycin A-induced mitochondrial damage was able to evoke a caspase-1-dependent inflammasome activation and the subsequent secretion of IL-1β and IL-18 in ARPE-19 and D407 cells. In agreement with our findings, a previous study has indicated that antimycin A induces the activation of the inflammasome as well as the secretion of IL-1β in macrophages (Zhou et al., 2010b).

All AMD-related studies this far have focused only on the role of the NLRP3 inflammasome. Previously, NLRP3 has been found abundant in the RPE of AMD patients when compared to age-matched controls (Tarallo et al., 2012; Tseng et al., 2013). For example, the A2E component of lipofuscin, *Alu* RNA, dysfunctional protein clearance, and oxidative stress have been shown to activate NLRP3 inflammasome in RPE cells (Anderson et al., 2013; Kauppinen et al., 2012; Piippo et al., 2014; Tarallo et al., 2012). In the present study, we found that antimycin A-induced mitochondrial damage triggers inflammasome activation, which was dependent on both NLRP3 and AIM2 inflammasomes. Previous studies have shown that mtROS (Heid et al., 2013; Nakahira et al., 2011; Zhou et al., 2010b) and cytosolic mtDNA (Shimada et al., 2012) can activate the NLRP3 inflammasome in macrophages. Nakahira et al. (2011) demonstrated that mtDNA release was critical for the assembly of the NLRP3 inflammasome and it was dependent on mtROS generation (Nakahira et al., 2011). Although the amount of mtDNA was not measured in the present study, it has previously been shown that mitochondrial damage leads to mtDNA release into cytosol (Nakahira et al., 2011; Shimada et al., 2012) also in RPE cells (Kerur et al., 2018). However, the role of NLRP3 detected in the present study is not surprising considering its vast and numerous activators, e.g. ATP (Mariathasan et al., 2006), K^+ efflux (Pétrilli et al., 2007), ROS production (Zhou et al., 2010a), and lysosomal damage (Hornung et al., 2008).

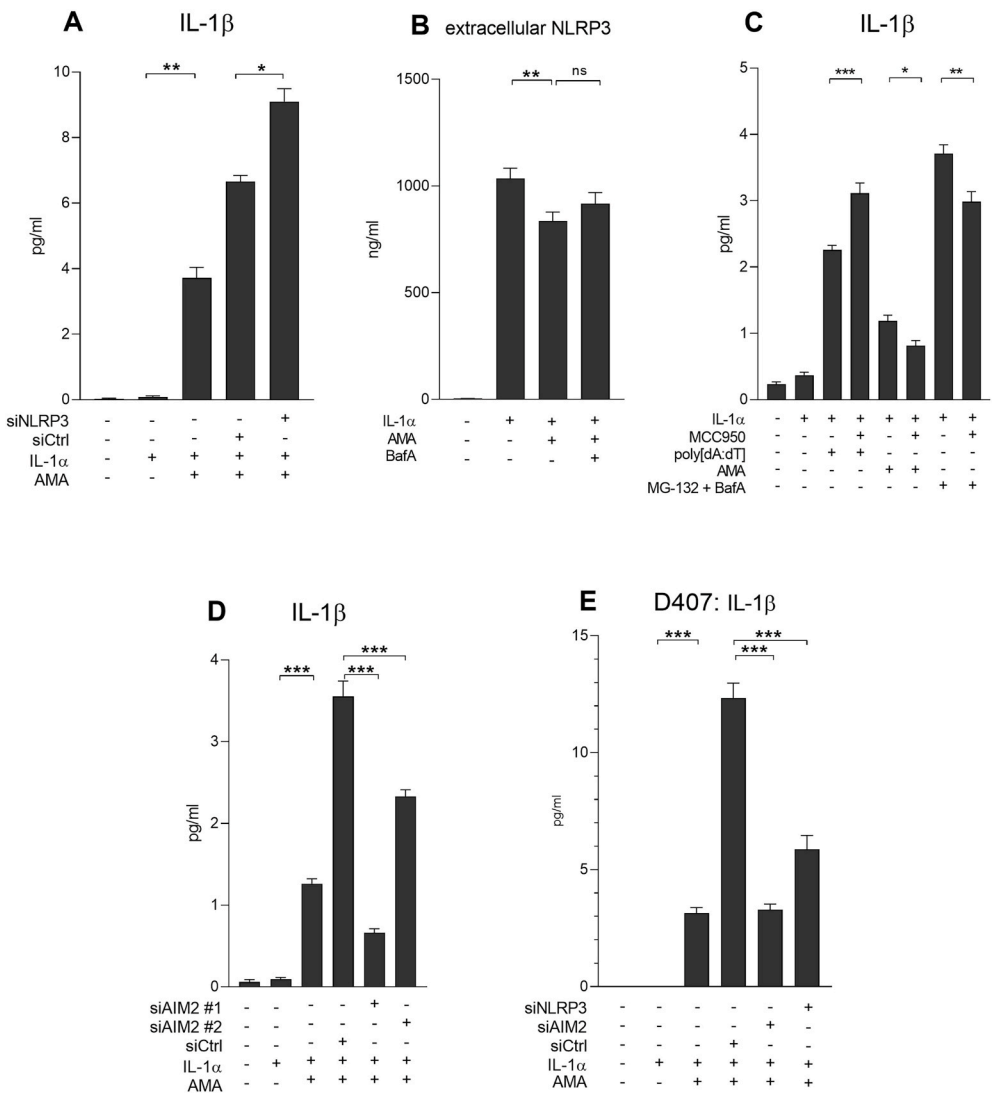

Fig. 5. Antimycin A induces NLRP3 and AIM2 inflammasome activation in ARPE-19 and D407 cells. Cells were transfected with NLRP3 siRNA for 24 h and primed with IL-1α (4 ng/ml) for the next 24 h. IL-1β was measured from the cell culture medium samples using the ELISA method 24 h after the antimycin A (25 μM) exposure (A). IL-1β data were combined from two independent experiments with six parallel samples in each group (A). Similarly, NLRP3 levels were measured from cell culture medium samples 24 h after the antimycin A exposure using the ELISA method (B). Bafilomycin A (50 nM) was added 1 h prior to the antimycin A exposure where applicable (B). NLRP3 ELISA data were combined from three independent experiments with 3–4 parallel samples in each group (B). Alternatively, ARPE-19 cells were treated with the NLRP3 inhibitor MCC950 (50 μM) either 1 h before the poly(dA:dT) or antimycin A or along with the MG-132 (5 μM) exposure (C). Bafilomycin A was added 24 h after the MG-132 treatment where applicable (C). IL-1β was measured from cell culture medium samples 24 h after the addition of the last activator (C). Data from these experiments were combined from three independent experiments with four parallel samples in each group (C). Lastly, AIM2 knockdown with two distinct AIM2 siRNAs, #1 (s18092) or #2 (s18094), was performed 24 h prior to the priming with IL-1α (4 ng/ml) for 24 h followed by an exposure to antimycin A (25 μM) (D). IL-1β was measured from the cell culture medium samples 24 h after the antimycin A exposure using the ELISA method and data were combined from three independent experiment with four parallel samples in each group (D). D407 cells were transfected as mentioned above, and IL-1α (4 ng/ml)-primed cells were exposed to antimycin A (12.5 μM; E). IL-1β was measured from cell culture medium samples 24 h after the antimycin A exposure using the ELISA method and data were combined from three independent experiment with four parallel samples in each group (E). All data from all the experiments (A–E) were presented as mean ± SEM and analyzed using Mann-Whitney *U* test. $^{*)}$ $p < 0.05$, $^{**)}$ $p < 0.01$, $^{***)}$ $p < 0.001$, $^{ns)}$ not significant. siCtrl = non-specific siRNA, siAIM2 #1 = AIM2 siRNA s18092, siAIM2 #2 = AIM2 siRNA s18094, AMA = antimycin A, BafA = bafilomycin A.

Despite the characteristic complex activation mechanism of NLRP3, it has been observed that the sensor protein of AIM2 directly recognizes dsDNA via electrostatic interactions (Jin et al., 2012) and cytosolic double-stranded DNA (dsDNA) fragments are well-known activators of the AIM2 inflammasome (Sharma et al., 2019; Kumari et al., 2020). It has previously been reported that endogenous mtDNA is capable of triggering AIM2 inflammasome activation in human keratinocytes (Dombrowski et al., 2012) as well as in activated BMDMs with an excessively high cholesterol content (Dang et al., 2017). As several previous studies have found that mtDNA activates either NLRP3 or AIM2, Shimada et al. (2012) demonstrated that the responsible inflammasome receptor is selected on whether mtDNA is oxidized. Although the oxidized form of mtDNA is able to activate both of these receptors, it seems that the oxidized form of mtDNA preferably activates NLRP3 whereas the unoxidized form of mtDNA leads to AIM2 activation (Shimada et al., 2012). In line with that proposal, 8-OH-dG has been demonstrated to be an oxidized DNA molecule which is recognized by NLRP3 (Zhong et al., 2018). On the other hand, responsible inflammasome receptor activated by cytosolic DNA may be dependent on the cell type (Gaidt et al., 2017). Gaidt et al. found that cytosolic DNA led to cGAS-STING-mediated NLRP3 inflammasome activation in human primary monocytes, whereas the same inflammasome activator induced the activation of AIM2 in THP-1 cells (Gaidt et al., 2017). Thirdly, it has to be taken into consideration that both NLRP3 and AIM2 inflammasomes can be activated in a single cell after the one danger signal. Cunha et al. showed that the assembly of AIM2 inflammasome through the active but unprocessed caspase-1 triggered subsequent NLRP3 inflammasome activation in the same cell after BMDMs were exposed to *Legionella pneumophila* (Cunha et al., 2017). A *legionella pneumophila* infection resulted in the assembly of two distinct inflammasome complexes in the same cell (Cunha et al., 2017), whereas *Aspergillus fumigatus* infection formed a cytoplasmic inflammasome platform consisting of both AIM2 and NLRP3 (Karki et al. 2015). Therefore, these previous studies are in line with our present data, which show that mitochondrial damage induces the activation of both NLRP3 and AIM2 in human RPE cells.

Although NLRP3 knockdown had a negligible effect on the antimycin A-induced production of IL-1β in ARPE-19 cells, the association of NLRP3 with the antimycin A-induced inflammasome activation was confirmed by NLRP3 siRNA and NLRP3 inhibitor MCC950 on antimycin A-exposed D407 and ARPE-19 cells, respectively. Our present data showed that NLRP3 knockdown efficiently reduced the production of IL-1β in antimycin A-induced D407 cells. In ARPE-19 cells, NLRP3 inflammasome activation was inhibited by MCC950, which is a widely used indicator of NLRP3 activation that directly interacts with the NACHT domain of NLRP3 (Coll et al., 2019). This interaction blocked ATP hydrolysis and inhibited the assembly of NLRP3 inflammasome multiprotein complex (Coll et al., 2019). Regardless of the involvement of NLRP3 inflammasome activation in antimycin A-induced ARPE-19 and D407 cells, we also detected mildly reduced extracellular levels of NLRP3 after antimycin A exposure. In agreement with that finding, Jabaut and colleagues have earlier presented that antimycin A could reduce the levels of inflammasome components in cell lysates of macrophages from serum amyloid A-exposed mice (Jabaut et al., 2013). However, the aforementioned treatment augmented the extracellular levels of pro-IL-1β, NLRP3 and IL-1β (Jabaut et al., 2013). Another study showed that antimycin A pre-treatment reduced NLRP3 and IL-1β gene induction in LPS-treated BMDMs, and extracellular IL-1β production in LPS and nigericin-treated BMDMs (Martínez-García et al., 2019). Moreover, antimycin A has reduced the production of extracellular IL-1β in ATP-exposed BMDMs but not in nigericin or R837-exposed BMDMs (Sadatomi et al., 2017). In contrast, Nomura and colleagues showed that it is the diminished levels of intracellular ATP, which activate NLRP3 inflammasome in human and murine macrophages (Nomura et al., 2015). In line with that result, antimycin A reduced intra- and extracellular levels of ATP in serum amyloid A-treated mouse macrophages (Jabaut et al., 2013). Interestingly, it is also known that ATP levels are reduced in the RPE of AMD donors when compared to RPE cells of healthy controls (Ferrington et al., 2017; Golestaneh et al., 2017). Although some ATP can also be synthesized via glycolytic pathway (Melkonian and Schury, 2020), it appears that inflammasome activation is evidently dependent on the altered levels of ATP generated in mitochondria, and this may act as a basis for future studies investigating the involvement of ATP-gated P2X7 receptors in human RPE cells and in the pathogenesis of AMD. Recently, the activation of P2X7 receptor was shown to induce mitochondrial depolarization, swelling, and ROS production in resting monocytes and macrophages (Martínez-García et al., 2019).

Interestingly, we found in the present study that the production of IL-18 was independent of NLRP3 but dependent on AIM2 in antimycin A-induced RPE cells. We have recently shown that IL-18 secretion occurs independently of NLRP3 in UVB-irradiated ARPE-19 cells (Korhonen et al., 2020). In our previous study, IL-1β production was dependent on K^+ efflux but independent of ROS production, whereas the IL-18 secretion was dependent on ROS generation and independent of K^+ efflux (Korhonen et al., 2020). When studying the mechanism of antimycin A-induced inflammasome activation, we found that the secretion of IL-1β is mediated by ROS production in antimycin A-exposed ARPE-19 cells. This result is in agreement with the previous work done with macrophages (Zhou et al., 2010b). The ETC complex III is the main location of ROS generation in mitochondria (Chen et al., 2003) and blocking this site by antimycin A induces mtROS production (Chen et al., 2003; Zhou et al., 2010b; Piskernik et al., 2008). According to our present data, antimycin A treatment induced IL-1β production via both mitochondrial and NADPH oxidase-mediated ROS generation in ARPE-19 cells. The transmembrane subunit and NADPH oxidase regulator, p22phox, was upregulated after exposure to antimycin A. An increased expression of p22phox has recently been reported in the RPE of AMD patients when compared to healthy controls (Terluk et al., 2019). Additionally, mitochondrial oxidative stress has been shown to cause RPE dysfunction in SOD2 knockout mice (Brown et al., 2019). As mitochondria and NADPH oxidase are two major cellular ROS sources, they interact with each other and the activation of one pathway can activate the other (Dikalov, 2011). For example, increased mtROS and impaired levels of cytosolic Ca^{2+} by dysfunctional mitochondria have previously been shown to contribute to the activation of NADPH oxidase in human lymphoblasts and whole blood (Dikalov et al., 2012).

Moreover, we showed here that while the antimycin-A-induced inflammasome activation was dependent on the ROS production, it was independent of K^+ efflux. Although K^+ efflux has been closely linked to the activation of NLRP3 inflammasome (Pétrilli et al., 2007; Muñoz-Planillo et al., 2013), it is not obligatory for the assembly of the inflammasome complex. Similarly to the present study, we have previously shown that the decline in intracellular clearance was able to induce NLRP3 inflammasome activation in RPE cells and that this phenomenon was mechanistically ROS-dependent and K^+ efflux independent (Piippo et al., 2018a). In addition, two small-molecule ligands, imiquimod and CL097, activated NLRP3 inflammasome and the subsequent secretion of IL-1β via K^+ efflux-independent but ROS-dependent mechanism in murine bone-marrow derived dendritic cells (BMDCs) and BMDMs (Groβ et al., 2016). Imiquimod and CL097 target the mitochondrial ETC complex I and reduce cellular ATP levels similarly to the mitochondrial ETC complex I inhibitor, rotenone (Groβ et al., 2016). Additionally, exposure to another small molecule, GB111-NH_2, induced mitochondrial ROS-dependent and K^+ efflux-independent mechanism of NLRP3 activation in BMDMs (Sanman et al., 2016). Therefore, both the K^+ efflux-independent and dependent activation of the NLRP3 inflammasome can be explained by a dispersed trans-Golgi network, which has recently been shown to trigger the assembly of NLRP3 inflammasome even in situations with no K^+ efflux (Chen and Chen, 2018).

In conclusion, the AIM2 inflammasome played a major role in the production of IL-1β and IL-18 in antimycin A-induced mitochondrial damage model of human RPE cells. Antimycin A activated inflammasomes in ROS-dependent but K^+ efflux independent mechanism. Both mitochondria and NADPH oxidase were involved in the ROS-mediated production of IL-1β. In comparison to AIM2, NLRP3 had a minor role in the mitochondrial damage-induced IL-1β and negligible effect on IL-18 production in these ARPE-19 and D407 cells. Although the melanin binding of antimycin A limits the usage of antimycin A on highly pigmented primary RPE cells, this study points out a novel role of AIM2 in the pathology of AMD and highlights the crucial role of mitochondria in the regulation of inflammation. To our knowledge, this is the first study showing the AIM2 inflammasome activation as a result from mitochondrial damage in human RPE cells.

Authors' contributions

E.K. and A.K. conceived and designed the study; E.K., M.H., and N.P. performed the experiments; E.K. analyzed the data; A.K. and K.K. contributed to materials and analytical tools; E.K. and A.K. wrote the paper, and others critically reviewed, commented, and provided suggestions to the manuscript.

Declaration of competing interest

The authors declare no conflict of interest.

Acknowledgements

The authors wish to thank Prof. Heli Skottman for providing hESC-RPE cells, and PhD Laura Hellinen for the preparation and generous gift of the melanin microparticles. Dr. Ewen MacDonald is warmly acknowledged for language revision and Res. Dir. Emeritus Antero Salminen for valuable discussions and critical review of the manuscript. This study was financially supported by the Mary and Georg C. Ehrnrooth Foundation, the Paulo Foundation, the Academy of Finland (Health Research Council projects AK297267, AK307341, AK328443), the Päivikki and Sakari Sohlberg Foundation, the Finnish Cultural

Foundation – North Savo Regional Fund, and the Emil Aaltonen Foundation.

Appendix A. Supplementary data

Supplementary data to this article can be found online at https://doi.org/10.1016/j.exer.2021.108687.

References

Anderson, O.A., Finkelstein, A., Shima, D.T., 2013. A2E induces IL-1ß production in retinal pigment epithelial cells via the NLRP3 inflammasome. PloS One 8, e67263. https://doi.org/10.1371/journal.pone.0067263.

Augsburger, F., Filippova, A., Rasti, D., Seredenina, T., Lam, M., Maghzal, G., Mahiout, Z., Jansen-Dürr, P., Knaus, U.G., Doroshow, J., Stocker, R., Krause, K., Jaquet, V., 2019. Pharmacological characterization of the seven human NOX isoforms and their inhibitors. Redox Biol 26, 101272. https://doi.org/10.1016/j.redox.2019.101272.

Bae, J.H., Jo, S., Kim, S.J., Lee, J.M., Jeong, J.H., Kang, J.S., Cho, N., Kim, S.S., Lee, E.Y., Moon, J., 2019. Circulating cell-free mtDNA contributes to AIM2 inflammasome-mediated chronic inflammation in patients with type 2 diabetes. Cells 8, 328. https://doi.org/10.3390/cells8040328.

Banoth, B., Cassel, S.L., 2018. Mitochondria in innate immune signaling. Transl. Res.: J. Lab. Clin. Med. 202, 52–68. https://doi.org/10.1016/j.trsl.2018.07.014.

Barreau, E., Brossas, J.Y., Courtois, Y., Treton, J.A., 1996. Accumulation of mitochondrial DNA deletions in human retina during aging. Invest. Ophthalmol. Vis. Sci. 37, 384–391.

Bradford, M.M., 1976. A rapid and sensitive method for the quantitation of microgram quantities of protein utilizing the principle of protein-dye binding. Anal. Biochem. 72, 248–254. https://doi.org/10.1006/abio.1976.9999.

Brown, E.E., DeWeerd, A.J., Ildefonso, C.J., Lewin, A.S., Ash, J.D., 2019. Mitochondrial oxidative stress in the retinal pigment epithelium (RPE) led to metabolic dysfunction in both the RPE and retinal photoreceptors. Redox Biol. 24, 101201. https://doi.org/10.1016/j.redox.2019.101201.

Chen, J., Chen, Z.J., 2018. PtdIns4P on dispersed trans -Golgi network mediates NLRP3 inflammasome activation. Nature 564, 71–76. https://doi.org/10.1038/s41586-018-0761-3.

Chen, Q., Vazquez, E.J., Moghaddas, S., Hoppel, C.L., Lesnefsky, E.J., 2003. Production of reactive oxygen species by mitochondria CENTRAL ROLE OF COMPLEX III. J. Biol. Chem. 278, 36027–36031. https://doi.org/10.1074/jbc.M304854200.

Christgen, S., Place, D.E., Kanneganti, T., 2020. Toward targeting inflammasomes: insights into their regulation and activation. Cell Res. 30, 315–327. https://doi.org/10.1038/s41422-020-0295-8.

Coll, R.C., Hill, J.R., Day, C.J., Zamoshnikova, A., Boucher, D., Massey, N.L., Chitty, J.L., Fraser, J.A., Jennings, M.P., Robertson, A.A.B., Schroder, K., 2019. MCC950 directly targets the NLRP3 ATP-hydrolysis motif for inflammasome inhibition. Nat. Chem. Biol. 15, 556–559. https://doi.org/10.1038/s41589-019-0277-7.

Cunha, L.D., Silva, A.L.N., Ribeiro, J.M., Mascarenhas, D.P.A., Quirino, G.F.S., Santos, L. L., Flavell, R.A., Zamboni, D.S., 2017. AIM2 engages active but unprocessed caspase-1 to induce noncanonical activation of the NLRP3 inflammasome. Cell Rep. 20, 794–805. https://doi.org/10.1016/j.celrep.2017.06.086.

Dang, E.V., McDonald, J.G., Russell, D.W., Cyster, J.G., 2017. Oxysterol restraint of cholesterol synthesis prevents AIM2 inflammasome activation. Cell 171, 1057–1071. https://doi.org/10.1016/j.cell.2017.09.029 e11.

Dib, B., Lin, H., Maidana, D.E., Tian, B., Miller, J.B., Bouzika, P., Miller, J.W., Vavvas, D. G., 2015. Mitochondrial DNA has a pro-inflammatory role in AMD. Biochim. Biophys. Acta 1853, 2897–2906. https://doi.org/10.1016/j.bbamcr.2015.08.012.

Dikalov, S., 2011. Crosstalk between mitochondria and NADPH oxidases. Free Radic. Biol. Med. 51, 1289–1301. https://doi.org/10.1016/j.freeradbiomed.2011.06.033.

Dikalov, S.I., Li, W., Doughan, A.K., Blanco, R.R., Zafari, A.M., 2012. Mitochondrial reactive oxygen species and calcium uptake regulate activation of phagocytic NADPH oxidase. Am. J. Physiol. Regul. Integr. Comp. Physiol. 302, R1134–R1142. https://doi.org/10.1152/ajpregu.00842.2010.

Dombrowski, Y., Peric, M., Koglin, S., Kaymakanov, N., Schmezer, V., Reinholz, M., Ruzicka, T., Schauber, J., 2012. Honey bee (Apis mellifera) venom induces AIM2 inflammasome activation in human keratinocytes. Allergy 67, 1400–1407. https://doi.org/10.1111/all.12022.

Fernandes-Alnemri, T., Yu, J., Wu, J., Datta, P., Alnemri, E.S., 2009. AIM2 activates the inflammasome and cell death in response to cytoplasmic DNA. Nature 458, 509–513. https://doi.org/10.1038/nature07710.

Ferrington, D.A., Ebeling, M.C., Kapphahn, R.J., Terluk, M.R., Fisher, C.R., Polanco, J.R., Roehrich, H., Leary, M.M., Geng, Z., Dutton, J.R., Montezuma, S.R., 2017. Altered bioenergetics and enhanced resistance to oxidative stress in human retinal pigment epithelial cells from donors with age-related macular degeneration. Redox Biol. 13, 255–265. https://doi.org/10.1016/j.redox.2017.05.015.

Fisher, C.R., Ferrington, D.A., 2018. Perspective on AMD pathobiology: a bioenergetic crisis in the RPE. Invest. Ophthalmol. Vis. Sci. 59, AMD41–AMD47. https://doi.org/10.1167/iovs.18-24289.

Gaidt, M.M., Ebert, T.S., Chauhan, D., Ramshorn, K., Pinci, F., Zuber, S., O'Duill, F., Schmid-Burgk, J.L., Hoss, F., Buhmann, R., Wittmann, G., Latz, E., Subklewe, M., Hornung, V., 2017. The DNA inflammasome in human myeloid cells is initiated by a STING-cell death program upstream of NLRP3. Cell 171, 1110–1124. https://doi.org/10.1016/j.cell.2017.09.039 e18.

Golestaneh, N., Chu, Y., Xiao, Y., Stoleru, G.L., Theos, A.C., 2017. Dysfunctional autophagy in RPE, a contributing factor in age-related macular degeneration. Cell Death Dis. 8, e2537 https://doi.org/10.1038/cddis.2016.453.

Groß, C.J., Mishra, R., Schneider, K.S., Médard, G., Wettmarshausen, J., Dittlein, D.C., Shi, H., Gorka, O., Koenig, P., Fromm, S., Magnani, G., Ćiković, T., Hartjes, L., Smollich, J., Robertson, A.A.B., Cooper, M.A., Schmidt-Supprian, M., Schuster, M., Schroder, K., Broz, P., Traidl-Hoffmann, C., Beutler, B., Kuster, B., Ruland, J., Schneider, S., Perocchi, F., Groß, O., 2016. K+ efflux-independent NLRP3 inflammasome activation by small molecules targeting mitochondria. Immunity 45, 761–773. https://doi.org/10.1016/j.immuni.2016.08.010.

Handa, J.T., Bowes Rickman, C., Dick, A.D., Gorin, M.B., Miller, J.W., Toth, C.A., Ueffing, M., Zarbin, M., Farrer, L.A., 2019. A systems biology approach towards understanding and treating non-neovascular age-related macular degeneration. Nat. Commun. 10 https://doi.org/10.1038/s41467-019-11262-1, 3347-11.

Heid, M.E., Keyel, P.A., Kamga, C., Shiva, S., Watkins, S.C., Salter, R.D., 2013. Mitochondrial ROS induces NLRP3-dependent lysosomal damage and inflammasome activation. J. Immunol. 191, 5230–5238. https://doi.org/10.4049/jimmunol.1301490.

Hellinen, L., Bahrpeyma, S., Rimpelä, A., Hagström, M., Reinisalo, M., Urtti, A., 2020. Microscale thermophoresis as a screening tool to predict melanin binding of drugs. Pharmaceutics 12. https://doi.org/10.3390/pharmaceutics12060554.

Hornung, V., Ablasser, A., Charrel-Dennis, M., Bauernfeind, F., Horvath, G., Caffrey, D. R., Latz, E., Fitzgerald, K.A., 2009. AIM2 recognizes cytosolic dsDNA and forms a caspase-1 activating inflammasome with ASC. Nature 458, 514–518. https://doi.org/10.1038/nature07725.

Hornung, V., Bauernfeind, F., Halle, A., Samstad, E.O., Kono, H., Rock, K.L., Fitzgerald, K.A., Latz, E., 2008. Silica crystals and aluminum salts mediate NALP-3 inflammasome activation via phagosomal destabilization. Nat. Immunol. 9, 847–856. https://doi.org/10.1038/ni.1631.

Hytti, M., Korhonen, E., Hyttinen, J.M.T., Roehrich, H., Kaarniranta, K., Ferrington, D.A., Kauppinen, A., 2019. Antimycin A-induced mitochondrial damage causes human RPE cell death despite activation of autophagy. Oxid Med Cell Longev, 1583656. https://doi.org/10.1155/2019/1583656, 2019.

Jabaut, J., Ather, J.L., Taracanova, A., Poynter, M.E., Ckless, K., 2013. Mitochondria-targeted drugs enhance Nlrp3 inflammasome-dependent IL-1β secretion in association with alterations on cellular redox and energy status. Free Radic. Biol. Med. 60, 233–245. https://doi.org/10.1016/j.freeradbiomed.2013.01.025.

Jin, T., Perry, A., Jiang, J., Smith, P., Curry, J.A., Unterholzner, L., Jiang, Z., Horvath, G., Rathinam, V., Johnstone, R.W., Hornung, V., Latz, E., Bowie, A.G., Fitzgerald, K.A., Xiao, T.S., 2012. Structures of the HIN domain:DNA complexes reveal ligand binding and activation mechanisms of the AIM2 inflammasome and IFI16 receptor. Immunity 36, 561–571. https://doi.org/10.1016/j.immuni.2012.02.014.

Kaarniranta, K., Uusitalo, H., Blasiak, J., Felszeghy, S., Kannan, R., Kauppinen, A., Salminen, A., Sinha, D., Ferrington, D., 2020. Mechanisms of mitochondrial dysfunction and their impact on age-related macular degeneration. Prog. Retin. Eye Res., 100858 https://doi.org/10.1016/j.preteyeres.2020.100858.

Karki, R., Man, S.M., Malireddi, R.K.S., Gurung, P., Vogel, P., Lamkanfi, M., Kanneganti, T., 2015. Concerted activation of the AIM2 and NLRP3 inflammasomes orchestrates host protection against Aspergillus infection. Cell Host Microbe 17, 357–368. https://doi.org/10.1016/j.chom.2015.01.006.

Karunadharma, P.P., Nordgaard, C.L., Olsen, T.W., Ferrington, D.A., 2010. Mitochondrial DNA damage as a potential mechanism for age-related macular degeneration. Invest. Ophthalmol. Vis. Sci. 51, 5470–5479. https://doi.org/10.1167/iovs.10-5429.

Kauppinen, A., Paterno, J.J., Blasiak, J., Salminen, A., Kaarniranta, K., 2016. Inflammation and its role in age-related macular degeneration. Cell. Mol. Life Sci. 73, 1765. https://doi.org/10.1007/s00018-016-2147-8.

Kauppinen, A., Niskanen, H., Suuronen, T., Kinnunen, K., Salminen, A., Kaarniranta, K., 2012. Oxidative stress activates NLRP3 inflammasomes in ARPE-19 cells–implications for age-related macular degeneration (AMD). Immunol. Lett. 147, 29–33. https://doi.org/10.1016/j.imlet.2012.05.005.

Kerur, N., Fukuda, S., Banerjee, D., Kim, Y., Fu, D., Apicella, I., Varshney, A., Yasuma, R., Fowler, B.J., Baghdasaryan, E., Marion, K.M., Huang, X., Yasuma, T., Hirano, Y., Serbulea, V., Ambati, M., Ambati, V.L., Kajiwara, Y., Ambati, K., Bastos-Carvalho, A., Ogura, Y., Terasaki, H., Oshika, T., Kim, K.B., Hinton, D.R., Leitinger, N., Cambier, J. C., Buxbaum, J.D., Kenney, M.C., Jazwinski, S.M., Nagai, H., Hara, I., West, A.P., Fitzgerald, K.A., Sadda, S.R., Gelfand, B.D., Ambati, J., 2018. cGAS drives non-canonical inflammasome activation in age-related macular degeneration. Nat. Med. 24, 50–61. https://doi.org/10.1038/nm.4450.

Korhonen, E., Piippo, N., Hytti, M., Hyttinen, J.M.T., Kaarniranta, K., Kauppinen, A., 2020. Only IL-1β release is inflammasome-dependent upon ultraviolet B irradiation although IL-18 is also secreted. Faseb. J. 34, 6437–6448. https://doi.org/10.1096/fj.201902355RR.

Korhonen, E., Piippo, N., Hytti, M., Hyttinen, J.M.T., Kaarniranta, K., Kauppinen, A., 2019. SQSTM1/p62 Regulates the Production of IL-8 and MCP-1 in IL-1β-stimulated Human Retinal Pigment Epithelial Cells, vol. 116. Cytokine, Philadelphia, Pa, pp. 70–77. https://doi.org/10.1016/j.cyto.2018.12.015.

Kumari, P., Russo, A.J., Shivcharan, S., Rathinam, V.A., 2020. AIM2 in health and disease: inflammasome and beyond. Immunol. Rev. 297, 83–95. https://doi.org/10.1111/imr.12903.

Lefevere, E., Toft-Kehler, A.K., Vohra, R., Kolko, M., Moons, L., Van Hove, I., 2017. Mitochondrial dysfunction underlying outer retinal diseases. Mitochondrion 36, 66–76. https://doi.org/10.1016/j.mito.2017.03.006.

Li, J.Q., Welchowski, T., Schmid, M., Mauschitz, M.M., Holz, F.G., Finger, R.P., 2019. Prevalence and incidence of age-related macular degeneration in Europe: a systematic review and meta-analysis. Br. J. Ophthalmol. 104 https://doi.org/10.1136/bjophthalmol-2019-314422 bjophthalmol-1084.

Malik, A., Kanneganti, T., 2017. Inflammasome activation and assembly at a glance. J. Cell Sci. 130, 3955. https://doi.org/10.1242/jcs.207365.

Mariathasan, S., Weiss, D.S., Newton, K., McBride, J., O'Rourke, K., Roose-Girma, M., Lee, W.P., Weinrauch, Y., Monack, D.M., Dixit, V.M., 2006. Cryopyrin activates the inflammasome in response to toxins and ATP. Nature 440, 228–232. https://doi.org/10.1038/nature04515.

Martínez-García, J.J., Martínez-Banaclocha, H., Angosto-Bazarra, D., de Torre-Minguela, C., Baroja-Mazo, A., Alarcón-Vila, C., Martínez-Alarcón, L., Amores-Iniesta, J., Martín-Sánchez, F., Ercole, G.A., Martínez, C.M., González-Lisorge, A., Fernández-Pacheco, J., Martínez-Gil, P., Adriouch, S., Koch-Nolte, F., Luján, J., Acosta-Villegas, F., Parrilla, P., García-Palenciano, C., Pelegrin, P., 2019. P2X7 receptor induces mitochondrial failure in monocytes and compromises NLRP3 inflammasome activation during sepsis. Nat. Commun. 10, 2711. https://doi.org/10.1038/s41467-019-10626-x.

Melkonian, E.A., Schury, M.P., 2020. Biochemistry, anaerobic glycolysis. In: Anonymous StatPearls. StatPearls Publishing, Treasure Island (FL.

Muñoz-Planillo, R., Kuffa, P., Martínez-Colón, G., Smith, B.L., Rajendiran, T.M., Núñez, G., 2013. K+ efflux is the common trigger of NLRP3 inflammasome activation by bacterial toxins and particulate matter. Immunity 38, 1142–1153. https://doi.org/10.1016/j.immuni.2013.05.016.

Nakahira, K., Haspel, J.A., Rathinam, V.A., Lee, S., Dolinay, T., Lam, H.C., Englert, J.A., Rabinovitch, M., Cernadas, M., Kim, H.P., Fitzgerald, K.A., Ryter, S.W., Choi, A.M., 2011. Autophagy proteins regulate innate immune response by inhibiting NALP3 inflammasome-mediated mitochondrial DNA release. Nat. Immunol. 12, 222. https://doi.org/10.1038/ni.1980.

Nomura, J., So, A., Tamura, M., Busso, N., 2015. Intracellular ATP decrease mediates NLRP3 inflammasome activation upon nigericin and crystal stimulation. J. Immunol. 195, 5718–5724. https://doi.org/10.4049/jimmunol.1402512.

Orning, P., Lien, E., Fitzgerald, K.A., 2019. Gasdermins and their role in immunity and inflammation. J. Exp. Med. 216, 2453. https://doi.org/10.1084/jem.20190545.

Pétrilli, V., Papin, S., Dostert, C., Mayor, A., Martinon, F., Tschopp, J., 2007. Activation of the NALP3 inflammasome is triggered by low intracellular potassium concentration. Cell Death Differ. 14, 1583–1589. https://doi.org/10.1038/sj.cdd.4402195.

Piippo, N., Korhonen, E., Hytti, M., Kinnunen, K., Kaarniranta, K., Kauppinen, A., 2018a. Oxidative stress is the principal contributor to inflammasome activation in retinal pigment epithelium cells with defunct proteasomes and autophagy. Cell. Physiol. Biochem. 49, 359–367. https://doi.org/10.1159/000492886.

Piippo, N., Korhonen, E., Hytti, M., Skottman, H., Kinnunen, K., Josifovska, N., Petrovski, G., Kaarniranta, K., Kauppinen, A., 2018b. Hsp90 inhibition as a means to inhibit activation of the NLRP3 inflammasome. Sci. Rep. 8 https://doi.org/10.1038/s41598-018-25123-2.

Piippo, N., Korkmaz, A., Hytti, M., Kinnunen, K., Salminen, A., Atalay, M., Kaarniranta, K., Kauppinen, A., 2014. Decline in cellular clearance systems induces inflammasome signaling in human ARPE-19 cells. Biochim. Biophys. Acta Mol. Cell Res. 1843, 3038–3046. https://doi.org/10.1016/j.bbamcr.2014.09.015.

Piskernik, C., Haindl, S., Behling, T., Gerald, Z., Kehrer, I., Redl, H., Kozlov, A.V., 2008. Antimycin A and lipopolysaccharide cause the leakage of superoxide radicals from rat liver mitochondria. Biochim. Biophys. Acta (BBA) - Mol. Basis Dis. 1782, 280–285. https://doi.org/10.1016/j.bbadis.2008.01.007.

Qiu, Y., Tao, L., Lei, C., Wang, J., Yang, P., Li, Q., Lei, B., 2015. Downregulating p22phox ameliorates inflammatory response in Angiotensin II-induced oxidative stress by regulating MAPK and NF-κB pathways in ARPE-19 cells. Sci. Rep. 5, 14362 https://doi.org/10.1038/srep14362.

Sadatomi, D., Nakashioya, K., Mamiya, S., Honda, S., Kameyama, Y., Yamamura, Y., Tanimura, S., Takeda, K., 2017. Mitochondrial function is required for extracellular ATP-induced NLRP3 inflammasome activation. J. Biochem. 161, 503–512. https://doi.org/10.1093/jb/mvw098.

Sanman, L.E., Qian, Y., Eisele, N.A., Ng, T.M., van der Linden, Wouter, A., Monack, D.M., Weerapana, E., Bogyo, M., 2016. Disruption of glycolytic flux is a signal for inflammasome signaling and pyroptotic cell death. eLife 5, e13663. https://doi.org/10.7554/eLife.13663.

Sharma, B.R., Karki, R., Kanneganti, T., 2019. Role of AIM2 inflammasome in inflammatory diseases, cancer and infection. Eur. J. Immunol. 49, 1998–2011. https://doi.org/10.1002/eji.201848070.

Shimada, K., Crother, T.R., Karlin, J., Dagvadorj, J., Chiba, N., Chen, S., Ramanujan, V. K., Wolf, A.J., Vergnes, L., Ojcius, D.M., Rentsendorj, A., Vargas, M., Guerrero, C., Wang, Y., Fitzgerald, K.A., Underhill, D.M., Town, T., Arditi, M., 2012. Oxidized mitochondrial DNA activates the NLRP3 inflammasome during apoptosis. Immunity 36, 401–414. https://doi.org/10.1016/j.immuni.2012.01.009.

Tarallo, V., Hirano, Y., Gelfand, B., Dridi, S., Kerur, N., Kim, Y., Cho, W., Kaneko, H., Fowler, B., Bogdanovich, S., Albuquerque, R.C., Hauswirth, W., Chiodo, V., Kugel, J., Goodrich, J., Ponicsan, S., Chaudhuri, G., Murphy, M., Dunaief, J., Ambati, B., Ambati, J., Ogura, Y., Yoo, J., Lee, D., Provost, P., Hinton, D., Núñez, G., Baffi, J., Kleinman, M., 2012. DICER1 loss and Alu RNA induce age-related macular degeneration via the NLRP3 inflammasome and MyD88. Cell 149, 847–859. https://doi.org/10.1016/j.cell.2012.03.036.

Terluk, M.R., Kapphahn, R.J., Soukup, L.M., Gong, H., Gallardo, C., Montezuma, S.R., Ferrington, D.A., 2015. Investigating mitochondria as a target for treating age-related macular degeneration. J. Neurosci. 35, 7304–7311. https://doi.org/10.1523/jneurosci.0190-15.2015.

Terluk, M.R., Ebeling, M.C., Fisher, C.R., Kapphahn, R.J., Yuan, C., Kartha, R.V., Montezuma, S.R., Ferrington, D.A., 2019. N-Acetyl-L-cysteine protects human retinal pigment epithelial cells from oxidative damage: implications for age-related macular degeneration. Oxidative Med. Cell. Longevity 1–14. https://doi.org/10.1155/2019/5174957, 2019.

Tseng, W.A., Thein, T., Kinnunen, K., Lashkari, K., Gregory, M.S., D'Amore, P.A., Ksander, B.R., 2013. NLRP3 inflammasome activation in retinal pigment epithelial cells by lysosomal destabilization: implications for age-related macular degeneration. Invest. Ophthalmol. Vis. Sci. 54, 110. https://doi.org/10.1167/iovs.12-10655.

Vaajasaari, H., Ilmarinen, T., Juuti-Uusitalo, K., Rajala, K., Onnela, N., Narkilahti, S., Suuronen, R., Hyttinen, J., Uusitalo, H., Skottman, H., 2011. Toward the defined and xeno-free differentiation of functional human pluripotent stem cell-derived retinal pigment epithelial cells. Mol. Vis. 22 (17), 558–575.

Velez-Montoya, R., Oliver, S.C.N., Olson, J.L., Fine, S.L., Quiroz-Mercado, H., Mandava, N., 2014. Current Knowledge and Trends in Age-Related Macular Degeneration: Genetics, Epidemiology, and Prevention, vol. 34. Retina, Philadelphia, Pa, pp. 423–441. https://doi.org/10.1097/IAE.0000000000000036.

Wang, A.L., Lukas, T.J., Yuan, M., Neufeld, A.H., 2008. Increased mitochondrial DNA damage and down-regulation of DNA repair enzymes in aged rodent retinal pigment epithelium and choroid. Mol. Vis. 14, 644–651.

Wong, W.L., Su, X., Li, X., Cheung, C.M.G., Klein, R., Cheng, C., Wong, T.Y., 2014. Global prevalence of age-related macular degeneration and disease burden projection for 2020 and 2040: a systematic review and meta-analysis. Lancet Global Health 2, e106–e116. https://doi.org/10.1016/S2214-109X(13)70145-1.

Zheng, D., Liwinski, T., Elinav, E., 2020. Inflammasome activation and regulation: toward a better understanding of complex mechanisms. Cell Discov. 6, 36. https://doi.org/10.1038/s41421-020-0167-x.

Zhong, Z., Liang, S., Sanchez-Lopez, E., He, F., Shalapour, S., Lin, X., Wong, J., Ding, S., Seki, E., Schnabl, B., Hevener, A.L., Greenberg, H.B., Kisseleva, T., Karin, M., 2018. New mitochondrial DNA synthesis enables NLRP3 inflammasome activation. Nature 560, 198–203. https://doi.org/10.1038/s41586-018-0372-z.

Zhou, R., Tardivel, A., Thorens, B., Choi, I., Tschopp, J., 2010a. Thioredoxin-interacting protein links oxidative stress to inflammasome activation. Nat. Immunol. 11, 136–140. https://doi.org/10.1038/ni.1831.

Zhou, R., Yazdi, A.S., Menu, P., Tschopp, J., 2010b. A role for mitochondria in NLRP3 inflammasome activation. Nature (London) 469, 221–225. https://doi.org/10.1038/nature09663.